**Title**
Elliptically Polarizing Undulator End Designs



**Journal**
IEEE Transactions on Applied Superconductivity, 16(2)

**ISSN**
1051-8223

**Authors**
Schlueter, RD
Marks, S
Prestemon, S

**Publication Date**
2006-06-01

**DOI**
10.1109/tasc.2006.871311

Peer reviewed

# Elliptically Polarizing Undulator End Designs

Ross D. Schlueter, Steve Marks, and Soren Prestemon

***Abstract*—The magnetic end design of pure-permanent magnet Apple-II elliptically polarizing undulators (EPU) is discussed. Constraints on end block dimensions and positions are presented that guarantee steering and displacement free systems in both transverse directions and at all gaps for $\mu = 1$ material. For block material with $\mu > 1$ some beam steering (i.e. integrated dipole) may occur due to the ends; in particular, the integrated dipole strength varies with EPU phase. An optimization process is presented that assumes small perturbations about the $\mu = 1$ solution and minimizes the variation in steering with EPU phase. We present numerical and experimental results that quantify the reduction in integrated dipole variation with phase.**

***Index Terms*—Elliptically polarizing undulator, magnetic end design, permanent magnets.**

## I. Introduction

THE design of permanent magnet elliptically polarizing undulators (EPU) is a mature topic, with a large number of devices installed and operating on a variety of synchrotron rings. Successful algorithms and designs have been presented that minimize the beam steering impact of EPU's as users vary the field strength and polarization. The usual design approach is to define end block geometric degrees of freedom and minimize some figure of merit associated with the integrated steering under various polarization modes using finite element or boundary integral methods [1]–[3].

We propose a modified approach to EPU end design that also significantly reduces variations in the first integrals

$$I_{x,y} = \int_{-\infty}^{\infty} B_{x,y}(0,0,z)dz \tag{1}$$

(i.e. beam steering) as a function of quadrant-shift and gap, but that makes use of the fact that rare-earth permanent magnet material typically has relative anisotropic permeability that can reasonably be viewed as "small", i.e. $\mu_{||,\perp} = 1 + \varepsilon_{||,\perp}$, with $\varepsilon_{||,\perp} \ll 1$. The variation of $I_{x,y}$ is known to emanate from variation of the permeability of a block neighborhood at the ends, i.e., as rows are shifted some blocks will be surrounded by air rather than $\mu_{||}$ or $\mu_{\perp}$. Furthermore, the approach minimizes the impact of uncertainties in the actual anisotropic permeability of the permanent magnet material ends (NdBFe blocks typically have $\mu_{||} = 1.05$, $\mu_{\perp} = 1.15$, but these values may vary).

Manuscript received September 20, 2005. This work was supported by the U. S. Department of Energy, under Contract no. DE-AC02-05CH11231.

The authors are with the Lawrence Berkeley National Laboratory, Berkeley, CA USA (e-mail: rdschlueter@lbl.gov; s_marks@lbl.gov; soprestemon@lbl.gov).

Digital Object Identifier 10.1109/TASC.2006.871311

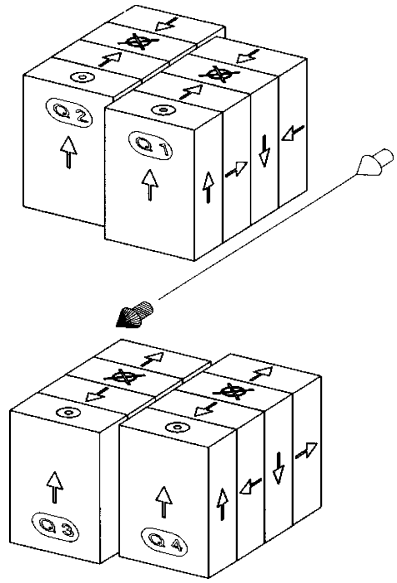


Fig. 1. Schematic of the EPU structure. As the rows shift, an end block will be subjected to variations in the neighboring permeability.

The original EPU end design is steering-free (and displacement free) for all phase shifts, assuming isotropic material with $\mu = 1.0$ for the blocks and no block errors ("ideal" device). The ideal device end design and associated geometric constraints on blocks are described in Section II. In Section III we outline the model used to optimize EPU ends taking into account anisotropic permeability of PM material. The modified design continues to satisfy the gap-independent steering (and displacement) free conditions for an ideal device, but optimizes geometric parameters within these constraints to minimize $I_{x,y}$ variations for "real" devices, i.e. taking into account nonunity permeability in the blocks.

## II. End Design for Unit Permeability Material

### A. Preliminary Concepts

Assume a passing electron encounters a magnetic field kick $K$ at a location $-z_0$, shown schematically in Fig. 1. The electron is deflected (steered) by an angle $\varphi(z) = K$, and is displaced by a distance $\delta(z) = K(z - z_0)$, as it progresses downstream. A second positive kick $K$ located at $z_0$ will increase the deflection angle to $\varphi(z) = 2K$; the displacement downstream of the kicks will behave as $\delta(z) = K(z - z_0) + K(z + z_0) = 2Kz$. More generally, the angle is the sum of the kicks; the displacement is a function of the sum of the kicks and of their centroid, but does not depend on the details of their distribution.

The kick associated with a permanent magnet block of an EPU structure can be easily evaluated analytically using

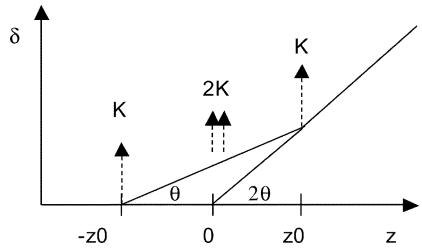


Fig. 2. Schematic of the impact of a magnetic kick on the trajectory of a passing electron. A kick results in net steering of a passing electron. The net effect downstream of multiple kicks is additive, centered on the total kick centroid.

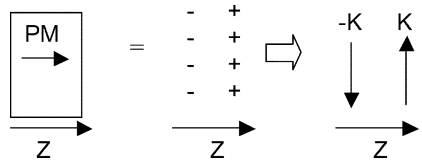


Fig. 3. The field from a permanent magnet can be evaluated using the surface charge model. Each surface charge results in an effective kick to the electron. For a horizontally magnetized block there is no net steering, although the passing electron is displaced.

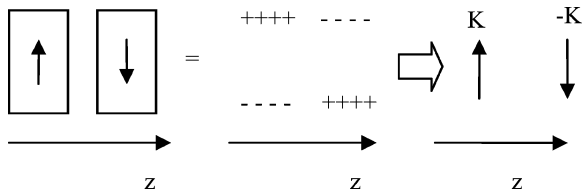


Fig. 4. The steering produced by a vertically magnetized block can be negated by a second block with opposite magnetization and equal length. The individual kick strength is proportional to the block length. Net displacement is proportional to block length and the spacing between the two blocks.

the charge sheet model [4], assuming $\mu = 1$ for the permanent magnet material. For magnetic material with constant $\vec{B}_r$ the kick imparted on the passing electrons is purely a function of the geometry. We restrict ourselves to rectangular blocks of Cartesian dimension $(\Delta x, \Delta y, \Delta z_i)$, where $z$ is parallel to the to the beam direction. For a horizontally magnetized block $\vec{B}_r = (0, 0, B_r)$ the kicks $K^{x1}$, $K^{y1}$ are inherently steering free (see Fig. 2), and a passing electron is displaced by $\delta^{x,y} = K^{x1,y1}\,\Delta z_i$. A vertically magnetized block $\vec{B}_r = (0, B_r, 0)$ will steer an electron by an angle $\varphi^{x,y} = K^{x2,y2}$. The diverse kick values can be computed analytically (see [1], [4]), but are not explicitly required here. The kick strength varies with the block location (i.e. gap), and this variation scales differently for horizontally and vertically magnetized blocks. The kicks associated with horizontally/vertically magnetized blocks are conceptually outlined in Figs. 3 and 4, respectively. It should be noted that the kick from a vertically polarized block is proportional to its longitudinal extent, i.e. $K^{x2,y2} \sim \Delta z_i$.

Using the analysis above it is clear that steering-free undulators are guaranteed if

$$\sum_{\text{i}\in\text{Vertical blocks}} K_i^{x2,y2} = 0 \tag{2}$$

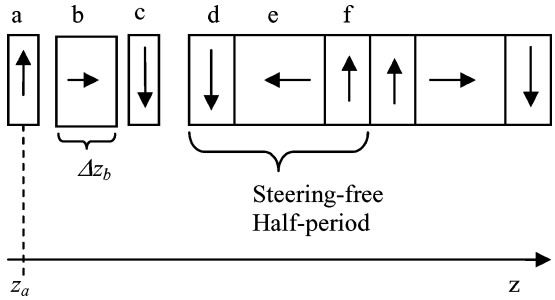


Fig. 5. Sketch of the end region of a planar undulator or APPLE-II EPU quadrant. The periodic section continues to the right.

An important result is that the precise relationship between K and $\varphi$, and its dependence on gap, is not required to generate steering-free ends.

Evaluation of the displacements of a series of blocks is also straightforward. For example

$$\delta_x(z) = \sum_{\text{i}\in\text{Vertical blocks}} K_i^{x2} H(z_i)(z - z_i) + \sum_{\text{i}\in\text{Hor. blocks}} K_i^{x1}\Delta z_i \tag{3}$$

where $\delta_x$ is the net x-displacement, $H$ is the Heaviside step function and $z_i$ is the axial center of the ith block.

### *B. Ideal Undulator Terminations*

The previous analysis implies that the periodic sections of permanent magnet undulators are steering free and displacement free, as expected. The ends will be steering free at all gaps if the $\pm$ vertical blocks are of the same length and the x and y block extents are identical. Fig. 5 provides a schematic of the end region of an undulator (or APPLE-II EPU quadrant).

An electron will be displaced by $\pm\delta_0$ as it progresses through each half-period of the periodic section. Ideal ends should therefore displace the electron by $\delta_{end} = \delta_0/2$, so that the transverse displacements occur symmetrically about the nominal particle trajectory. The kick strengths of the vertical and the horizontal blocks do not have the same dependence on distance from the electron, i.e. on the magnetic gap. It is therefore important to enforce geometric constraints for displacement independently for the two block types. Blocks d, e, f (see Fig. 5) are characteristic of the periodic section. For the ends the constraint on horizontal blocks to yield $\delta_{end} = \delta_0/2$ is then

$$K^{x1,y1}\Delta z_b = \frac{-K^{x1,y1}\Delta z_e}{2} \Rightarrow \Delta z_b = \frac{\Delta z_e}{2} \tag{4}$$

Note that the horizontal blocks are inherently steering-free.

For vertical blocks the constraint to yield $\delta_{end} = \delta_0/2$ can be written as

$$K_a^{x2,y2}(z_c - z_a) = \frac{-K_d^{x2,y2}(z_f - z_d)}{2} \Rightarrow -\frac{K_a^{x2,y2}}{K_d^{x2,y2}} = \frac{\frac{1}{2}(z_f - z_d)}{(z_c - z_a)} = \frac{\Delta z_a}{\Delta z_d} \tag{5}$$

Also, for steering free ends the constraint on vertical blocks is $\delta_a = \delta_c$.

The last equality in (5) stems from the linear dependence of kick on length. End configurations satisfying (4) and (5) are ideal, in the sense that for $\mu = 1$ material they are steering and displacement free for all gaps. In the case of an EPU structure, as shown in Fig. 1, such configurations can be applied to each quadrant, resulting in a steering and displacement free device at all gaps and in all polarization modes.

The simple relations in (4) and (5) allow for much flexibility. For instance (see Fig. 5):

1) Any individual vertical block can be split into multiple components arbitrarily positioned, provided their centroid remains the same;
2) The horizontal block can be positioned arbitrarily in the end section, and can even be segmented and distributed.

It is readily apparent that there is a large parameter space of end geometries satisfying (4) and (5). This space can be exploited to serve other purposes. For instance the total space occupied by the ends can be minimized, yielding a solution with no space between blocks, and

$$\Delta z_a = \left(\frac{\sqrt{7}-1}{2}\right)\frac{\lambda}{8}. \tag{6}$$

The original ALS EPU design [5] uses an end structure with no space between blocks and with the following end block sizes:

$$\begin{aligned}\frac{\Delta z_a}{\Delta z_d} &= 0.628\\ \frac{\Delta z_b}{\Delta z_e} &= 0.88\end{aligned} \tag{7}$$

Note that the size of block $b$ in (7) does not by itself satisfy (4); a second horizontal block $\overline{b}$ is therefore introduced, with negative horizontal magnetization and of size $\Delta z_{\overline{b}}/\Delta z_e = 0.38$, and located at the entrance to the device (see note 2 above). The configuration minimizes the entrance length needed to arrive at peak field amplitude, thereby maximizing the length over which coherent radiation can be generated.

## III. End Design Optimization for $\mu = 1 + \varepsilon$ Materials

The end design for the first ALS EPU's satisfies the constraints defined in (4) and (5). Integral measurements of the devices nevertheless show a row-phase dependence of integrated dipoles (1) as shown in Fig. 6. The variations are known to emanate from the variation in the neighboring permeability of the ends with quadrant-shift [2].

The geometry, including block lengths and positions, provide ample parameters to simultaneously satisfy the constraints in (4) and (5) and allow for further optimization to minimize variations in first integrals with row shifts that stem from variations in magnetic permeability. We define a figure of merit

$$F(\vec{p}) = \max_i |I_{x,y}(ds_i)| \tag{8}$$

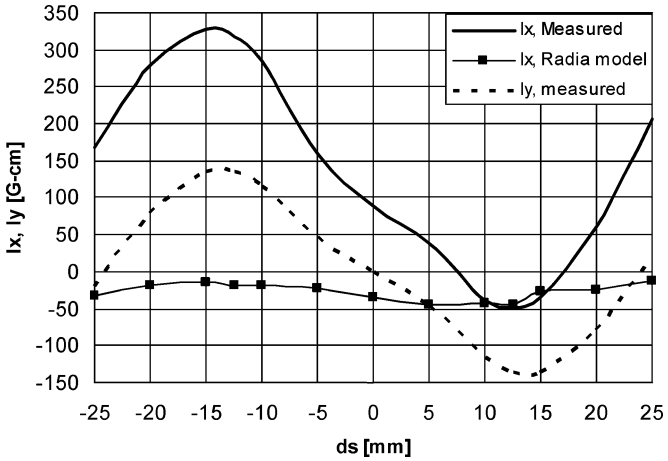


Fig. 6. Measured and calculated Ix(ds) curves for the existing EPU ends. The offset in the measured data is merely due to block and tolerance errors and can be corrected via virtual shimming.

TABLE I
Geometric Parameters Before and After Design Optimization

| Geometric Parameter | Original Design | Optimized Design |
|---|---|---|
| $\Delta z_a/\Delta z_d$ | 0.628 | 0.48 |
| $\Delta z_b/\Delta z_e$ | 0.88 | 0.74 |
| $\Delta z_{\overline{b}}/\Delta z_e$ | 0.38 | 0.24 |
| $\Delta z_c/\Delta z_d$ | 0.628 | 0.48 |
| $\Delta z_{\overline{b}a}/\Delta z_d$ | 0 | 0.16 |
| $\Delta z_{ab}/\Delta z_d$ | 0 | 0.445 |
| $\Delta z_{bc}/\Delta z_d$ | 0 | 0.72 |

where $\vec{p}$ is a vector in the parameter space satisfying (4) and (5). A discrete set of row shifts, defined in terms of the period length, can be chosen, e.g.

$$ds_i = 0, \frac{\lambda}{10}, \frac{2\lambda}{10}, \frac{\lambda}{4}, \frac{3\lambda}{10}, \frac{4\lambda}{10}, \frac{\lambda}{2}$$

The general algorithm is then

1) Determine a parameter space by specifying block length and position degrees of freedom.
2) Constrain the parameter space defined by (4) and (5); by providing four (or more) geometric degrees of freedom and applying (4) and (5), there will be two (or more) remaining degrees of freedom.
3) Discretize the remaining parameter space and evaluate the figure of merit (6) on each point.
4) The minimum $F(\vec{p})$ value yields the design point.

Applied to the EPU ends of an ALS EPU50, the algorithm results in a calculated reduction in the figure of merit $F(\vec{p}_{new})/F(\vec{p}_{old}) = 0.22$.

The magnetization-induced integrated dipole field can be calculated using Radia [1]. A 3-period undulator model reproduces the measured field and row-shift dependence very accurately (see Fig. 6). Parameters prior to and after optimization are shown in Table I. The calculated improvement (see Fig. 7) is similar in magnitude to that described in [2]. The optimized design continues to satisfy the steering and displacement-free

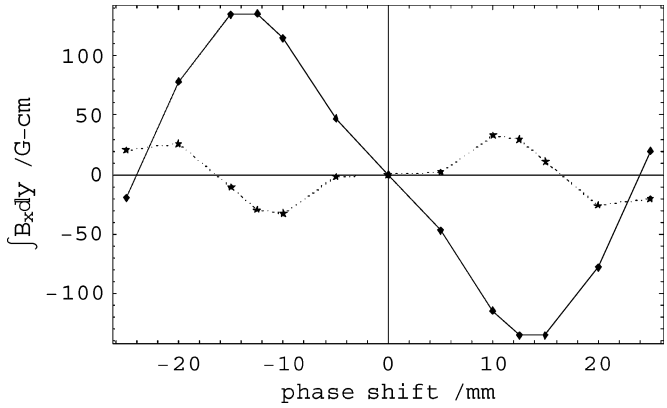


Fig. 7. Radia simulations of row-shift dependent first integral for an ALS EPU50 device before and after end termination optimization.

conditions of (4) and (5), but reduces the figure of merit (8) to 22% of its original value. Although slight further improvements (i.e. reduction in figure of merit, (8)) can be expected by investigating the full parameter space of geometric variables, the approach described in this paper decreases the parameter space by two degrees of freedom, resulting in significantly reduced computations.

## IV. Conclusion

The design of permanent magnet EPU ends that are steering-free and displacement-free at all gaps for $\mu = 1$ material is presented. Additional geometric parameters are available and can be used for further design optimization. We present an analysis approach that takes advantage of the small amplitude of the permeability in rare-earth permanent magnet material, resulting in an algorithm that takes into account magnetization effects while guaranteeing only small steering and displacement values under all operating conditions.

## Acknowledgment

The authors would like to thank David Robin and Christoph Steier for motivating the end design optimization study, and Oleg Chubar for help with using Radia.

## References

[1] P. Elleaume, O. Chubar, and J. Chavanne, "Computing 3D magnetic field from insertion devices," in *Proc. of the PAC97 Conference*, May 1997, pp. 3509–3511.

[2] J. Chavanne, P. Elleaume, and P. Van Vaerenbergh, "End field structure for linear/helical insertion devices," in *Proceedings of the 1999 Particle Accelerator Conference*, New York, 1999.

[3] S. C. Gottschalk, D. C. Quimby, and K. E. Robinson, "Zero-displacement end terminations of undulators and wigglers," in *Proc. of PAC*, NY, 1999.

[4] R. D. Schlueter and S. Marks, "Three dimensional pure permanent magnet undulator design theory," *IEEE Trans. on Magnetics*, vol. 32, no. 4, July 1996.

[5] S. Marks *et al.*, "The advanced light source elliptically polarizing undulator," in *Proc. 1997 PAC*, Vancouver, 1998, 3221.